



# A Powerful Nanocomposite Polymer Prepared From Metal Oxide Nanoparticles Synthesized *via* Brown Algae as Anti-corrosion and Anti-biofilm

Rawia F. Sadek<sup>1\*</sup>, Hala A. Farrag<sup>1</sup>, Shima M. Abdelsalam<sup>2</sup>, ZMH Keiralla<sup>2</sup>, Amany I. Raafat<sup>3</sup> and Eman Araby<sup>4</sup>

<sup>1</sup> Department of Drug Radiation Research, National Center for Radiation Research and Technology (NCRRT), Atomic Energy Authority, Egypt (AEA), Cairo, Egypt, <sup>2</sup> Botany Department, Faculty of Women for Arts, Science and Education, Ain Shams University, Cairo, Egypt, <sup>3</sup> Polymer Chemistry Department, National Center for Radiation Research and Technology (NCRRT), Atomic Energy Authority, Egypt (AEA), Cairo, Egypt, <sup>4</sup> Department of Radiation Microbiology, National Center for Radiation Research and Technology (NCRRT), Atomic Energy Authority, Egypt (AEA), Cairo, Egypt

## OPEN ACCESS

### Edited by:

Guang-Ling Song,  
Xiamen University, China

### Reviewed by:

Jingmao Zhao,  
Beijing University of Chemical  
Technology, China  
Dake Xu,  
Northeastern University, China

### \*Correspondence:

Rawia F. Sadek  
Rawiasadeck@yahoo.com

### Specialty section:

This article was submitted to  
Environmental Materials,  
a section of the journal  
Frontiers in Materials

Received: 17 February 2019

Accepted: 31 May 2019

Published: 02 July 2019

### Citation:

Sadek RF, Farrag HA, Abdelsalam SM, Keiralla Z, Raafat AI and Araby E (2019) A Powerful Nanocomposite Polymer Prepared From Metal Oxide Nanoparticles Synthesized *via* Brown Algae as Anti-corrosion and Anti-biofilm. *Front. Mater.* 6:140. doi: 10.3389/fmats.2019.00140

Chemical corrosion and bio-corrosion in water pipelines are the most common problem in the industry worldwide which cause damage to expensive equipment and increase the maintenance costs. In the current study, the nanocomposite composed of ZnO and CuO nanoparticles was successfully synthesized using brown algae (*Sargassum muticum*) extract and then dispersed in polyethylene oxide polymer. The synthesized nanoparticles were exposed to gamma radiation to reduce their particle size. The synthesized nanocomposites were characterized using UV-vis spectroscopy, Dynamic light scattering (DLS), X-ray diffraction (XRD), Transmission electron microscopy (TEM), and FTIR analysis, then, the anti-biofilm and anti-adherence efficacy of nanocomposite were evaluated. The results revealed that gamma radiation reduced the particle size of ZnO and CuO nanoparticles to 15 and 20 nm, respectively. Also, the results showed a significant reduction ( $P < 0.001$ ) in biofilm formation and adherence of *Proteus mirabilis* (*P. mirabilis*), *Pseudomonas aeruginosa* (*P. aeruginosa*), and *Staphylococcus aureus* (*S. aureus*) to carbon mild steel coupon C1010. In addition, from all the tested strains, *P. mirabilis* caused the highest bio-corrosion rate 1.5 mpy on mild steel coupon and nanocomposite prevented its adhesion as confirmed by Scanning electron microscope (SEM). Furthermore, the nanocomposite at 150 ppm showed the highest anti-corrosion activity 92.3% in 1 M HCl and exhibited mix-type inhibitor (cathodic and anodic). Finally, the results concluded that the green synthesized nanocomposite had multi-function to be used as anti-biofilm, bio-corrosion inhibitor, and anti-corrosion.

**Keywords:** green synthesis, CuO/ZnO nanocomposite polymer, anti-biofilm, anti-bio-corrosion, corrosion inhibitor, electrochemical impedance spectroscopy

## INTRODUCTION

Carbon mild steel C1010 is a preferred construction material in many industrial and domestic applications, including oil and gas pipelines, due to its good mechanical and chemical properties (Palazzo, 2016). Corrosion is a worldwide economic issue that is responsible for huge loss especially in the industrial sector (Little and Lee, 2014). The extensive damage of corrosion cost Egypt in 2013 was about \$98.25 billion USD (Paik and Melchers, 2014). There are different types of corrosive media at which the pipelines may suffer like salts (chloride salts), humidity or acids i.e., HCl causes a low pH system, which determines the corrosion degree of steel (Saab et al., 2005). Microbiologically Influenced Corrosion (MIC) is directly related to the presence and adherence of the microbes on industrial pipes subsequent metal deterioration and damage as a result of microbial activities that modify local chemistry at metal surfaces caused biocorrosion (Gu et al., 2019). Biofilm extracellular polysaccharide substance has sticky properties that aid the adherence to metal surfaces and protect bacterial elimination by biocides subsequently causing corrosion (Aruliah and Ting, 2014). The mixed culture biofilm type showed synergistic interaction. A biofilm formed by aerobic *Pseudomonas aeruginosa* encourages the formation of a locally oxygen free shelter that enhances the growth of *sulfate-reducing bacteria* (SRB) in an open-air system (Gu et al., 2019). That clarifies the high maintenance cost of open circuit water pipelines systems. Also the biofilm settles on the inside of the metal pipes causing clogging and reducing the pipe's diameter (Li et al., 2013; Vargas et al., 2017). To diminish the problem of corrosion either chemical or microbial, corrosion inhibitors are one of the common treatments. This includes cathodic, anodic protection, and surface treatments (Wei et al., 2013; Yeole et al., 2015). Many synthetic corrosion inhibitors are based on particular organic polymers which are used to provide long-lasting corrosion protection. Currently, the use of green synthesized nanomaterial as corrosion inhibitors has attracted the field of research as they can reduce or eliminate the use of the hazardous chemical substance, their natural origin, low cost, and efficiency (Sharma et al., 2008). The efficient green chemistry methods employing natural reducing, capping stabilizing agents to synthesized nanoparticles *via Sargassum muticum* brown algae is used for the green synthesis of nanoparticles as it contains various phenolic compounds, fucoidan, steroids, terpenoids, and flavonoids which act as reducing and stabilizing agents. Biological approach possesses non-toxic and cheap method compared to chemical synthesis approach. Moreover, they express active chemical groups (e.g., NH<sub>2</sub>, CO, and CHO) which are adsorbed on the metal surface to stimulate protection (Wang et al., 2006; Agarwal et al., 2017). The nanocomposites based on both inorganic nanoparticles and polymer can be prepared by the *ex-situ* approach. This method is carried out by dispersing the nanoparticles into a polymer matrix (Muñoz-Bonilla and Fernández-García, 2012). Nanocomposites were established excellent antibacterial activity depending on the nanoparticle size as this parameter changes the surface area that leads to better interaction with bacterial cells (Wang et al., 2017). The present study utilized the merits of nanotechnology for the development

of new corrosion and bio-corrosion inhibitors. Nanocomposite polymer (ZnO, CuO, and polyethylene oxide) prepared in eco-friendly. The nanocomposite was designed to have multi-function (anti-biofilm, anti-adherence, and anti-corrosion/bio-corrosion) to protect mild steel from bio-corrosion and corrosion in acidic media.

## MATERIALS AND METHODS

Brown algae (*Sargassum muticum*) were kindly provided from the Algal Laboratory of Ain Shams University which was collected from the Hurgada coast along the Red Sea, Egypt, and identified according to Aleem (1993). Zinc nitrate (Zn (NO<sub>3</sub>)<sub>2</sub>·6H<sub>2</sub>O); copper sulfate (CuSO<sub>4</sub>·5H<sub>2</sub>O) and Polyethylene oxide 5,000,000 Mwt linear formula (-CH<sub>2</sub>CH<sub>2</sub>O-) <sub>n</sub> were purchased from Sigma-Aldrich. Cobalt-60 gamma irradiation was performed at the National Center for Radiation Research and Technology, Atomic Energy Authority-Egypt.

### Green Synthesis of Nanocomposite

The brown algae sample was air dried for 3 days then ground to powder. Three grams of the dried powder was dissolved in 300 mL deionized water (dH<sub>2</sub>O) and stirred at 120°C for 30 min. The extract was filtered using Whatman paper No.1 and preserved at 5°C for 24 h. Exactly 70 mL of brown algae extract was added to 30 mL/0.1 mM metal salt solution (Zn (NO<sub>3</sub>)<sub>2</sub> and CuSO<sub>4</sub>) then the mixture was heated for 3 h with vigorous stirring. The color change was evident for the formation of nanoparticles. The prepared ZnO and CuO NPs were irradiated at 50 kGy and 100 kGy, respectively (dose rate of 1.73 kGy/h), to improve the particle size. For *ex-situ* nanocomposite formation, polyethylene oxide 5,000,000 Mwt, 0.8% wt. was dissolved in 100 mL of dH<sub>2</sub>O with vigorous stirring for 30 min. Afterward, equal volumes of the irradiated nanoparticles were dispersed with vigorous stirring at 70°C for 4 h then the formation of nanocomposite was characterized (Hanemann and Szabó, 2010; Tripathi et al., 2017).

### Physical Characterization

#### UV-Visible Spectroscopy (UV-vis)

The primary characterization of the nanoparticles was done using UV-visible spectroscopy (JASCO-Japan-model V- 560) at a resolution of 1 nm. Nanoparticles exhibit unique and tunable optical properties on the account of their surface Plasmon resonance (SPR) dependent on shape, size and size distribution of the nanoparticles. The reduction of metal ions was monitored by determining UV-visible spectra solutions from 200 to 800 nm.

#### Dynamic Light Scattering (DLS)

Average particle size and Nano-sized distribution were determined by DLS (PSS-NICOMP 380- ZLS, USA). Before measurements, the samples were diluted 10 times with deionized water. Exactly, 250 μL of the suspension was added to a disposable cuvette. Five measurements were performed using 12 runs of 10 s at a temperature of 25°C for 2 min.

### Fourier-Transform Infrared Spectroscopy (FTIR)

For FTIR, the tested sample was diluted with potassium bromide in the ratio of 1:100 and after drying (room temperature) compressed to form a disc. The disks were later subjected to FTIR spectroscopy. These measurements were recorded on a JA SCO FT-IR-3600 and the spectrum was collected at a resolution of  $4\text{ cm}^{-1}$  in wavenumber region of  $400\text{ cm}^{-1}$  to  $4,000\text{ cm}^{-1}$ . FT-IR measurements were done in order to obtain evidence about the chemical group.

### X-Ray Diffraction Patterns (XRD)

X-ray diffraction patterns of the nanocomposite was studied using XRD-diffractometer with Cu target. The XRD runs drive axis over  $2\theta$  with a scan range  $10\text{--}90^\circ$  at a Scan speed  $8.0000\text{ (deg/min)}$  sampling pitch  $0.02\text{ (deg)}$ .

### High-Resolution Transmission Electron Microscopy (TEM)

A high-resolution transmission electron microscopy image of the nanocomposite was directed at an accelerated voltage of 200 KV electron microscopes (JEM2100 LaB6, Japan). The dense sample was dispersed in ethanol solution *via* an ultrasonic and then dropped on a copper grid coated with carbon film prior to introducing the samples in the TEM column, the grid was vacuum dried for 15 min.

### Isolation, Purification, and Identification of Bacterial Isolates

Water was collected from different water pipelines. The water samples were taken using a sterile plastic bottle and then immediately transported to a laboratory for further investigation according to Eaton et al. (2005). The collected samples were inoculated in a selective medium, following the recommendations for field biological sampling, bacteria were isolated using standard methods. The media were used nutrient agar (Oxoid) as general media, MacConkey agar (Oxoid, No. 3) for Gram-negative bacteria, mannitol salt agar (Oxoid) for *Staphylococcus aureus* and cetrimide agar (Oxoid) for *Pseudomonas aeruginosa*. The plates were incubated aerobically at  $35^\circ\text{C}$  for 24 h. Presumptive pure colonies were subjected to specific preliminary and confirmatory biochemical tests. The obtained isolates were preserved using 15% glycerol and stored at  $4^\circ\text{C}$  for future use (Basu et al., 2015).

The analytical profile index (API) 20E **Supplementary Material** test was performed in accordance with the manufacturer's protocol (BioMérieux, Marcy l'Étoile, France). An API 20E strip was used to identify Gram-negative rods. Identification of *Staphylococcus aureus* species as well as to other species grouped under the general term of coagulase-negative *Staphylococci*. The API *Staph* code 20500 consists of a gallery containing the dehydrated substrate in their bottom for 19 different biochemical tests and one microtube as a negative control with no substrate. By using the API index (Specific index), the obtained number corresponds to the type of organisms (BioMérieux Co.) referring to the Analytical Profile Index or using the identification software.

### Biofilm Detection

Tissue culture plate assay (TCP) is considered as the standard test for the detection of biofilm formation. All strains were screened for their ability to form a biofilm, as described by TCP, which was done according to Mathur et al. (2006). For detecting strong biofilm producing strains, fresh pure cultures were inoculated in respective media (BHI Broth with 2% sucrose) and incubated for 24 h at  $37^\circ\text{C}$ . Then, 96 wells flat bottom microtiter culture plates were filled with  $200\text{ }\mu\text{L}$  ( $4.0 \times 10^8\text{ cells/mL}$ ) BHI broth and incubated for 48 h at  $37^\circ\text{C}$  diluted cultures individually.

### Nanocomposite Anti-bacterial and Minimum Inhibition Concentration

The determination of the antibacterial activity nanocomposite was performed according to Ruparella et al. (2008). The pure cultures of biofilm producer bacterial strains were used. The examined nanoparticles were tested *in vitro* for its antimicrobial activities against strains by the agar well diffusion technique. The determination of minimum inhibition concentration (MIC) of nanocomposite against bacterial strains using resazurin stain as an indicator for bacterial growth inhibition of tested nanocomposite materials according to Sarker et al. (2007).

### Anti-biofilm

To evaluate the anti-biofilm efficacy of nanocomposite; individual wells were filled with  $180\text{ }\mu\text{L}$  ( $4.0 \times 10^8\text{ cells/mL}$ ) BHI broth. Following that,  $10\text{ }\mu\text{L}$  of nanocomposite ( $35\text{ }\mu\text{g/mL}$ ) was inoculated in each well and incubated at  $37^\circ\text{C}$  for 48 h. Finally, the plates were determined with a micro-ELISA auto reader at wavelength  $620\text{ nm}$ . Each experiment was performed in triplicates. The average of OD values of the sterile medium (blank) was calculated and subtracted from all test values. The results were interpreted according to Stepanović et al. (2007).

### Hydrophobicity Assay

The bacterial adhesion to hydrocarbon (BATH) assay was performed according to Nakao et al. (2012). Exactly  $1\text{ mL}$  of toluene was added to  $1\text{ mL}$  of bacterial culture ( $6.4 \times 10^8\text{ cells/mL}$ ) with and without nanocomposite and vortexed for 2 min. The OD of the aqueous phase was measured after vortex and the percentage hydrophobicity was calculated using the formula:

$$\text{Hydrophobicity} = \left[ 1 - \frac{\text{OD600 after vortex}}{\text{OD600 before vortex}} \times 100 \right] \quad (1)$$

### Bio-Corrosion Studies and SEM Surface Analysis

In this experiment Carbon mild steel C1010 coupons were used to determine the bio-corrosive impact of the strongest biofilm producer strains.

### Coupons Preparation

Carbon mild steel C1010 coupons with chemical composition: (C = 0.10%, Mn = 0.45%, P = 0.04% max, S = 0.05% max) was purchased from Nippon Yakin Kogyo Co., Ltd., Japan. Coupons sizes ( $1 \times 1\text{ cm}$  and  $5\text{ mm}$  thickness) were polished with  $0.3\text{ }\mu\text{m}$  diamond paste to get a smooth mirror finish. Coupons were subsequently washed with plentiful water and finally rinsed with

70% ethanol (Wadood et al., 2015). Register each coupon weight as the initial weight. The prepared coupons were used for bio-corrosion evaluation and surface analysis using (weight loss method and SEM).

### Weight Loss Method

According to Aruliah and Ting (2014), twelve 250 mL conical flasks were prepared. Each flask contains a 100 mL sterile test water sample which was previously sterilized by autoclaving and inserted three pieces of prepared coupons. Then inoculated with 1 ml ( $8.0 \times 10^7$ ) of the tested strains which previously isolated from its water source. Each 7 days coupon was picked to examine its weight loss measurements. Average corrosion rate (mm/y). The control flask with 1% of nutrient liquid (Oxoid) without bacterial inoculation. At the end of bio-corrosion time, examine the strongest bio-corrosive strains that were selected and subjected to SEM analysis metal surface changes. The coupons were weighted at 7, 14, and 21 d to determine the weight loss and corrosion rate caused by each isolate. Bio-corrosion rate of the coupons was calculated in mils per year (mpy) following the equation proposed by ASTM standard as follows:

$$\text{Corrosion Rate (CR)} = \frac{W \cdot K}{(D) \cdot (A) \cdot (T)} \quad (2)$$

where:  $W$  = weight loss (g),  $K$  = Constant,  $D$  = density of the metal,  $\text{g/cm}^3$ ,  $A$  = exposed area of coupon,  $\text{cm}^2$ , and  $t$  = exposed time/days. The average weight loss and standard deviations (SD) were calculated via the SPSS virgin 20 statistical program (Batista et al., 2000; Moen et al., 2015).

The biofilm formation and inhibition on the C1010 carbon mild steel coupon were performed. Polished sterile coupons were immersed overnight in pure culture ( $4.0 \times 10^8$  cell/mL) with and without treatment with nanocomposite and incubated for different time intervals 18, 28, and 48 h. The biofilm on the coupon surface was fixed using 3% glutaraldehyde in a phosphate-buffered solution overnight and washed with ethanol

serially (25, 50, 75, 95% concentration) for SEM examination (Rajasekar et al., 2007).

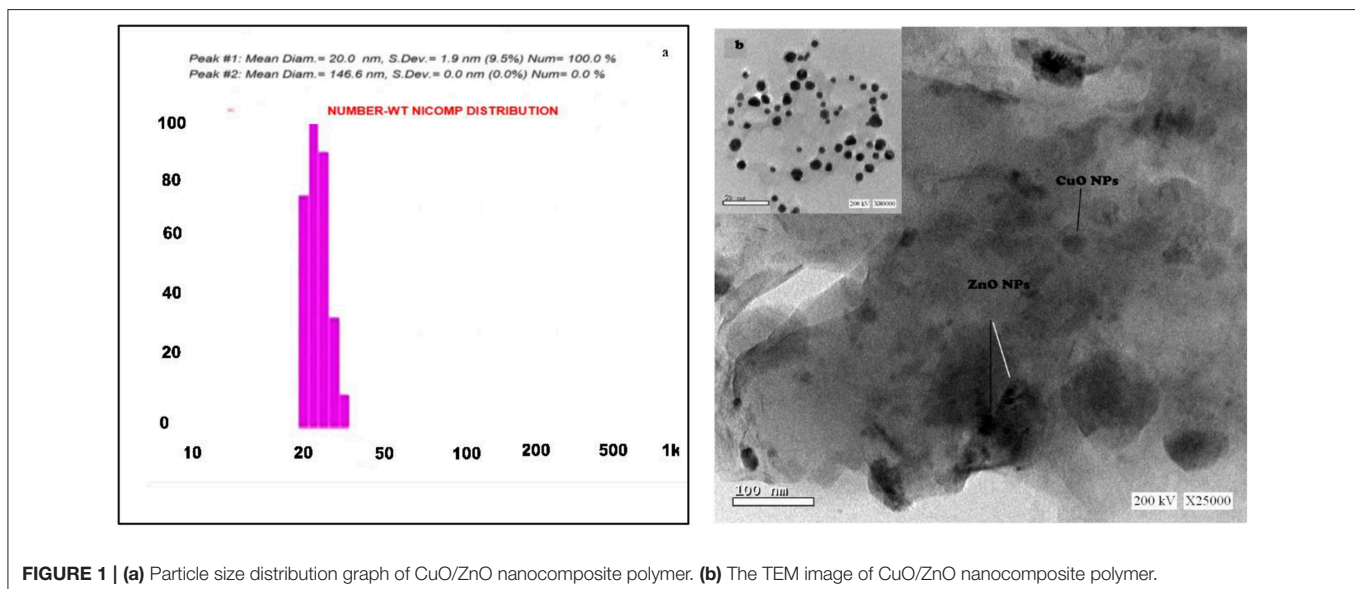
### Electrochemical Impedance Measurements (EIS)

Volta lab 80 (PGZ 402) potential with Volta master 4 software was used to carry out the potential-dynamic polarization and electrochemical impedance spectroscopy (EIS), at  $25^\circ\text{C}$  as a frequency response analyzer in a conventional three-electrode cell system. Mild steel specimens were acted as a working electrode (WE). A platinum electrode and saturated calomel electrode (SCE) acted as a counter electrode (CE) and a reference electrode (RE), respectively. The potential/current curves were obtained by sweeping the electrode potential at  $2 \text{ mVs}^{-1}$  from  $E_{\text{initial}} = -1,000 \text{ mV}$  to  $E_{\text{final}} = -200 \text{ mV}$ . EIS curves were obtained by employing frequency range was extended from 10 KHz to 10 MHz. Impedance tests were done in 1M HCl with and without nanocomposite inhibitor. Potential-dynamic polarization measurements were conducted with the same equipment used for impedance measurement leaving the frequency response analyzer out of consideration. Data were collected and analyzed using Corr-View, Corr-Ware, Z-plot software.

## RESULTS AND DISCUSSION

### Nanocomposite Characterization

The particle size of the formed nanocomposite using a one-step green method was in the range of 20–25 nm, measured by DLS as **Figure 1a** and TEM-images (**Figure 1b**) showed that the nanocomposite is clear, spherical in shape nanoparticles and was with the obtained DLS results. Control of the size and structure of the resultant nanoparticles can be related to the connections among bio-compounds and metal atoms (Azizi et al., 2013). The nanocomposite particle size as characterized



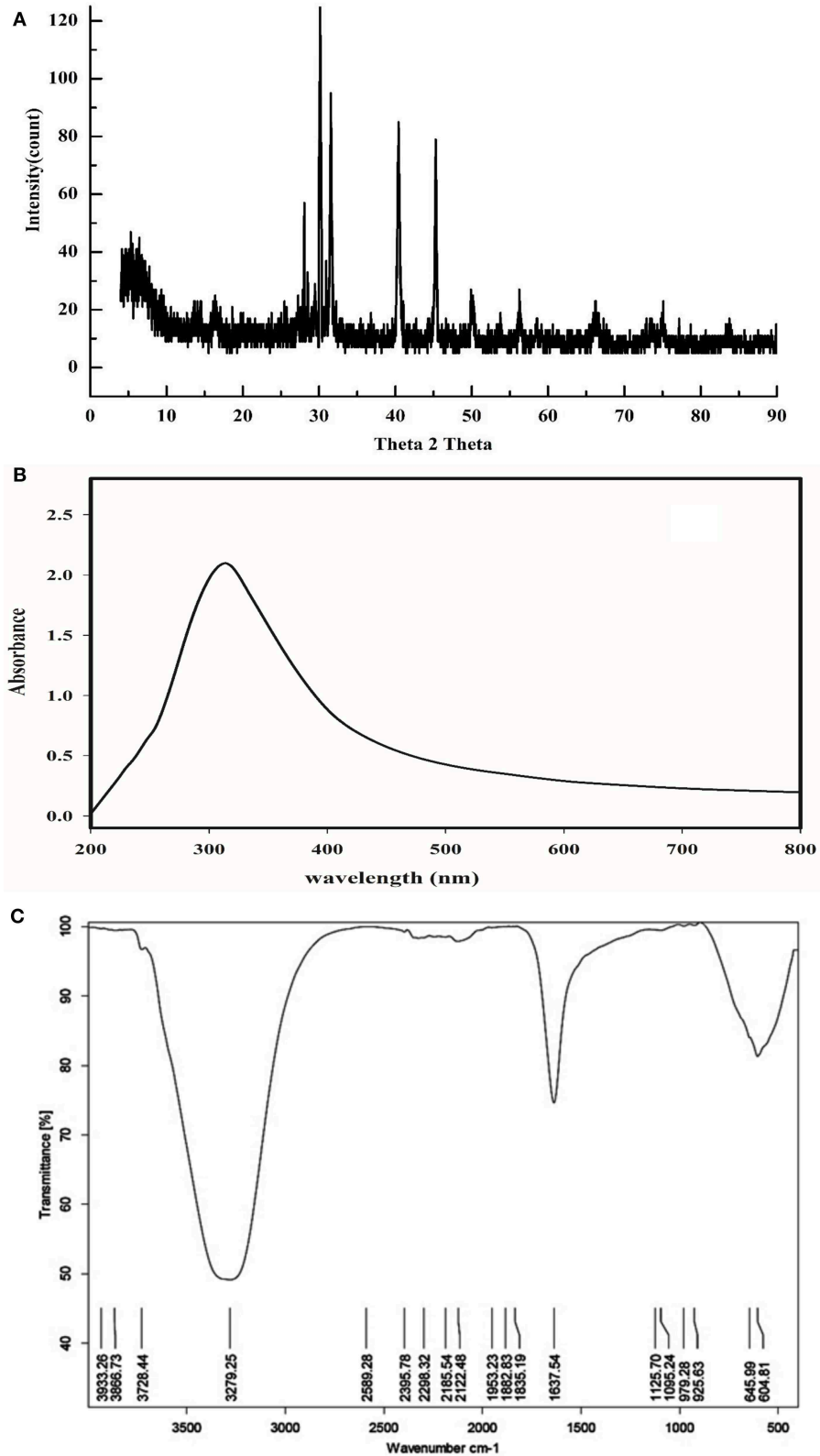


**FIGURE 2 | (A)** X-ray diffraction pattern of CuO/ZnO nanocomposite polymer. **(B)** UV-vis wavelength spectrum of CuO/ZnO nanocomposite polymer. **(C)** Fourier-transform infrared spectrum of CuO/ZnO nanocomposite polymer.

by UV-vis spectroscopy was found in the range of 250–450 nm (Figure 2B). CuO and ZnO nanoparticles displayed an absorption band in the range of 300–360 nm. The sharp absorption in the wavelength at 334 nm clarified the basic band absorption of ZnO/CuO crystals because of the electron transitions from the valence band to the conduction band (O2p-3d) associated with the surface plasmon resonance phenomena. In a nanostructure's aspect, the electronic states become completely discrete, as per atoms and molecules (Banik and Basumallick, 2017).

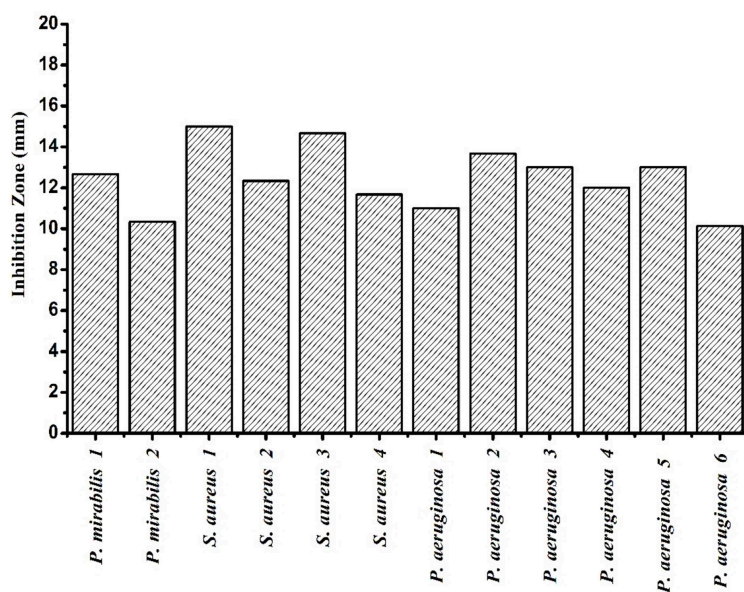
The XRD analysis of nanocomposite as shown in Figure 2A. The diffraction pattern has a high peak at 30, 34, 35, 40, 47, and 54°. The XRD patterns confirmed that ZnO and CuO nanostructures were crystallized and the prominent peak (101) for pure ZnO and (111) for pure CuO was selected as preferential orientation along the c-axis. These observations proved that; the basic crystal structure still the same, although a minor change in intensity is detected (Azmy et al., 2014). The nanocomposite presented high peak at 31, 34, 35, 47, 56, and 67°, ZnO peaks appeared at 31.7, 34.4, 36.2, 47.5, 56.5, 62.8, 67.9, and 69.05°. The CuO peak at 30–50° (Qamar et al., 2015). As shown in Figure 2C. The wavenumber of 432.05 cm<sup>-1</sup> is assigned to the Zn-O bond similar to the value reported by Chitra and Annadurai (2013). The wavenumber of 524.64 and 594.06 cm<sup>-1</sup> are assigned to the Cu-O bond according to Karthik et al. (2011). Peaks attributed to algae extract were also presented such as;  $\alpha$ ,  $\beta$ -unsaturated ketone C=O band at (1,730 cm<sup>-1</sup>), olefinic carbons (1,625 cm<sup>-1</sup>), primary and secondary alcohol (1,103 and 1,033 cm<sup>-1</sup>) as well as the peaks around 3,000 and 1,400 cm<sup>-1</sup> attributable to aliphatic C-H stretching and bending modes, respectively (Abboud et al., 2014).

## Isolation, Purification, and Identification of Bacteria

Out of 108 bacterial isolates from water pipelines 12 different phenotypic bacterial isolates were selected (four Gram positives and eight Gram negatives) based on their powerful biofilm production. Culturing on MacConkey, cetrimide agar, mannitol salt agar, and applying API revealed obtaining of two strains *Proteus mirabilis* (*P. mirabilis*), six strains *Pseudomonas aeruginosa* (*P. aeruginosa*), and four strains *Staphylococcus aureus* (*S. aureus*).

## Antimicrobial Activity of Nanocomposite

The antimicrobial activity of polymer composites based on CuO and ZnO nanoparticles have been much less studied than those based on silver (Palza, 2015). The prepared nanocomposite showed high antibacterial activity against the *S. aureus*1, *P. mirabilis*1, and *P. aeruginosa*2 than the rest of the bacterial strain as shown in Figure 3, this behavior of nanocomposite is related to synergism phenomena (Bogdanović et al., 2015). Moreover, the capability of polymers for long-term ion release extends the antibacterial activity of the nanocomposite. The Cu ions are able to kill bacteria cell, the copper surfaces also exhibit lethal effects through direct contact against bacteria (Faúndez et al., 2004). The ZnO NPs antibacterial activity during interaction with water, metal oxides produces reactive oxygen species (ROS) that are bacteria killer (Bikiaris and Triantafyllidis, 2013). The majority of bacterial strains were affected with minimum inhibition concentration of 7  $\mu$ g/mL and only two isolates *P. mirabilis*1 and *P. aeruginosa*3, 5 with 35  $\mu$ g/mL of nanocomposite (Figure 3).



Bacterial strains	MIC
<i>P. mirabilis</i> 1	35 $\mu$ g/mL
<i>P. mirabilis</i> 2	17 $\mu$ g/mL
<i>S. aureus</i> 1	17 $\mu$ g/mL
<i>S. aureus</i> 2	17 $\mu$ g/mL
<i>S. aureus</i> 3	17 $\mu$ g/mL
<i>S. aureus</i> 4	17 $\mu$ g/mL
<i>P. aeruginosa</i> 1	17 $\mu$ g/mL
<i>P. aeruginosa</i> 2	17 $\mu$ g/mL
<i>P. aeruginosa</i> 3	35 $\mu$ g/mL
<i>P. aeruginosa</i> 4	17 $\mu$ g/mL
<i>P. aeruginosa</i> 5	35 $\mu$ g/mL
<i>P. aeruginosa</i> 6	17 $\mu$ g/mL

**FIGURE 3** | Inhibition zone (mm) and minimum inhibition concentration (MIC)  $\mu$ g/ml of CuO/ZnO nanocomposite polymer against *Proteus mirabilis* (*P. mirabilis*), *Pseudomonas aeruginosa* (*P. aeruginosa*), and *Staphylococcus aureus* (*S. aureus*).

## Biocorrosion Index of Bacteria

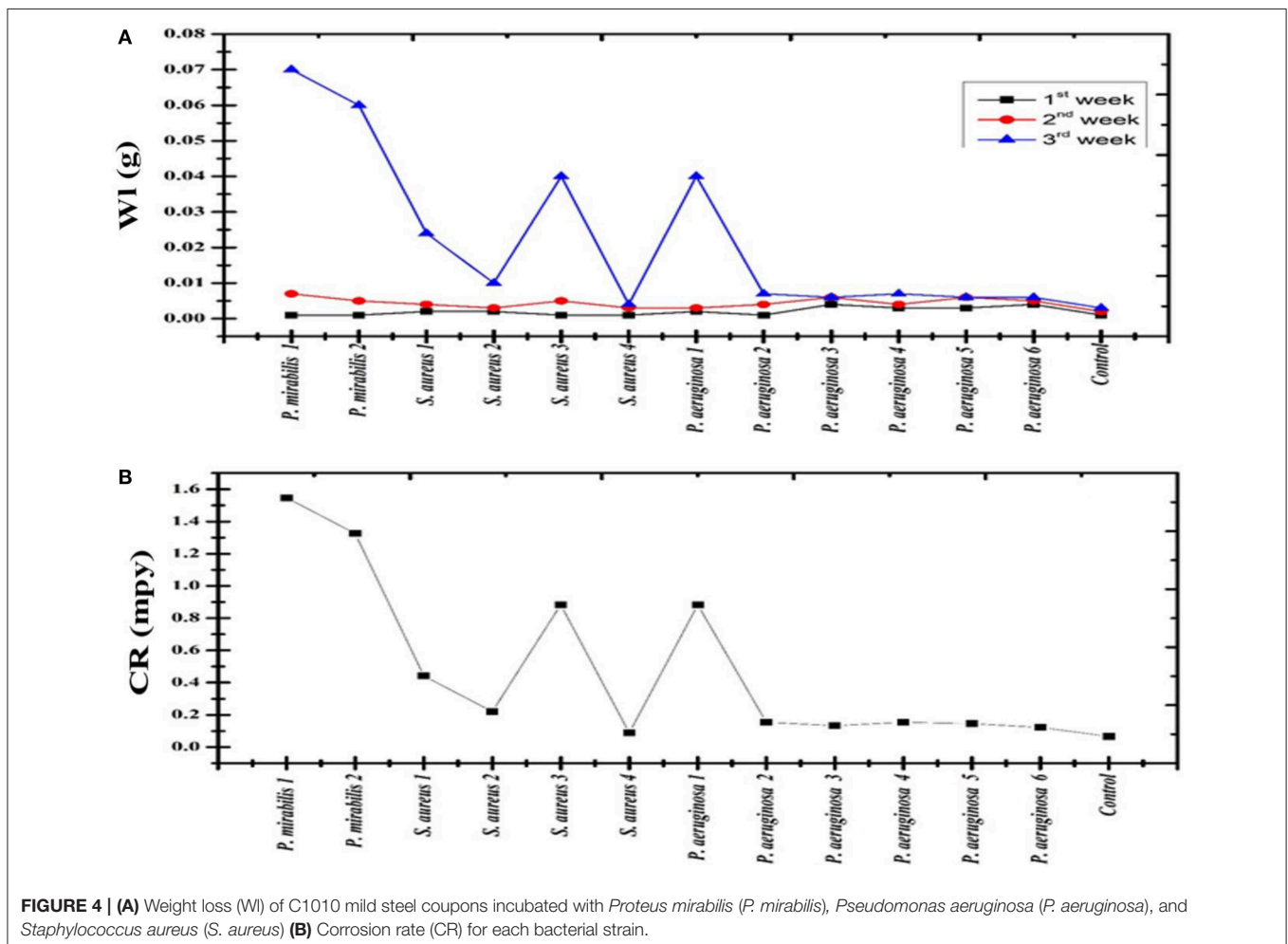
The data clarify that the highest biofilm and bio-corrosion rate occurred by *P. mirabilis*, *P. aeruginosa*, and *S. aureus* strains, respectively. *P. mirabilis*1 caused the highest bio-corrosion of the mild steel coupon with a rate of 1.535 mmpy which can be attributed to its ability to maintain enhanced local ion concentrations and/or by creating differential aeration area on the surface (Little and Lee, 2007). This finding was confirmed by SEM analysis for the mild steel coupon by observing the pores on its surface compared to the control (Figures 4A,B, 5). Also, it was observed that *P. mirabilis*.1 formed a biofilm layer which was detected by SEM (Figure 6). The areas under the biofilm can become oxygen depleted which increases the potential variation between the two sites, and subsequently causing the rapid corrosion of the coupon (Little et al., 1991; Jia et al., 2019).

The results in Figure 7 revealed that there was a significant reduction ( $P < 0.001$ ) in the biofilm formation with all tested strains after treatment with nanocomposite. Joshi et al. (2017) reported the reduction in the biofilm formation in *Salmonella typhi* can be attributed to the interaction between the bacterial cells and gold ion irradiated polycarbonate nanocomposite.

These results can be explained by the interference of the nanocomposite with the cell surface charge and reducing the extra-polysaccharide production, which is a very important phenomenon for biofilm development (Smith et al., 2010). Also, the polymer chain presented on the nanocomposite surface could create a tightly packed, highly hydrated brush in the aqueous environment that could repel the bacterial attachment causing biofilm eradication and it is a representative anti-corrosion coating (Chitra and Annadurai, 2013).

The efficiency of the nanocomposite may be referred to the passage of nanoparticles through the bacterial cell membrane then damaging the vital bacterial enzymes which eventually causes its death. Additionally, it was reported that the released copper ions can inhibit *P. aeruginosa*, *E. coli* and *S. aureus* biofilms (Nan et al., 2015; Sun et al., 2015; Lou et al., 2016).

Polymer hydrophobicity plays a crucial role in the adhesion of the bacterial cells and solid surfaces (Rosenberg and Rosenberg, 1985). The ability of bacteria to adhere strongly to hydrocarbons correlates to its attachment to the abiotic surface (Wang et al., 2015). So, the more hydrophobic bacteria are the stronger biofilm and the more bio-corrosive to the surface adhered on. The current study revealed that Gram-negative bacteria



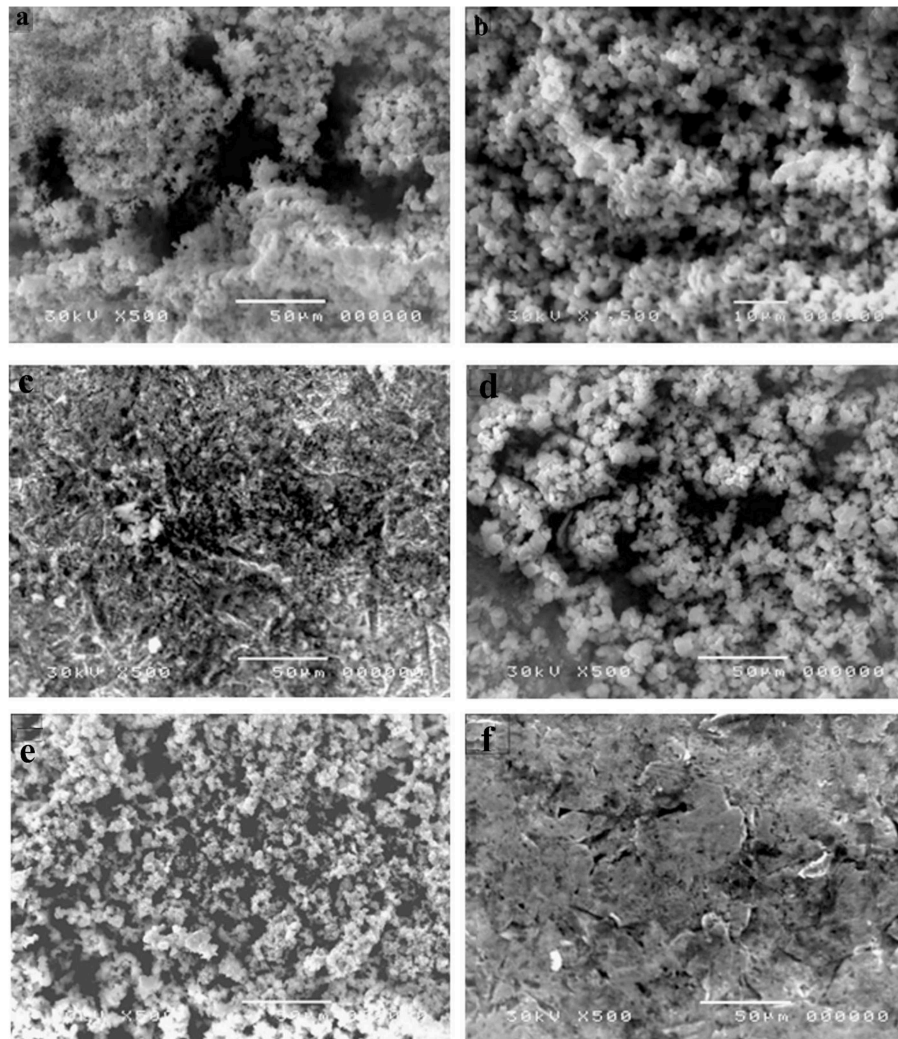


**FIGURE 5** | Bio-corrosion of different bacterial strains after 21 days **(a,c)** Coupon with *Pseudomonas aeruginosa*, **(b,d)** Coupon with *Staphylococcus aureus* **(e)** Coupon with *Proteus mirabilis* **(f)** Control; Coupon without bacteria.

*P. aeruginosa* and *P. mirabilis* are more hydrophobic when compared to Gram-positive bacteria *S. aureus*. The tested nanocomposite presented significant anti-hydrophobicity effects against *P. aeruginosa*, *P. mirabilis* and *S. aureus* as presented in **Table 1**. This can be explained by the release of outer membrane vesicles in Gram-negative bacteria causing a significant increase in cell surface hydrophobicity and enhanced biofilm formation (Baumgarten et al., 2012).

Energy dispersion spectrum (EDS) is the most popular technique used for examining and analyzing the elemental surface component of corrosion-related samples (Little and Lee, 2007). In **Figure 8** (EDS), was applied to determine the composition of mild steel coupon coating. A visible difference between the EDS of the coating with and without nanocomposite. The mild steel coupon surface revealed only C and O peaks. While the coupons treated with the nanocomposite showed C, Zn, O, and Cu peaks. The development of some primary Zn/Cu

single crystals in the areas coated by the nanocomposite. This result was in balance with previous studies (PraveenKumar et al., 2012; Aigbodion and Fayomi, 2016).

### Potential Dynamic Polarization

As showed in **Figure 9** the polarization curves were shifted directly to lower current densities and the corrosion rate of steel was decreased significantly with increasing the concentration of nanocomposite. This means that the hydrogen evolution and dissolution reactions of the tested mild steel electrode reactions are inhibited. The Tafel slope can be obtained by the Tafel extrapolation method as reported previously (Lgaz et al., 2017).

The nanocomposite polymer significantly boosted the anti-corrosive performance of such coatings on mild steel surfaces, as shown in **Table 2**. This table presents the calculated corrosion inhibition efficiency (IE%), the corrosion rate (CR) and the current density ( $i_{corr}$ ) were characteristically derived

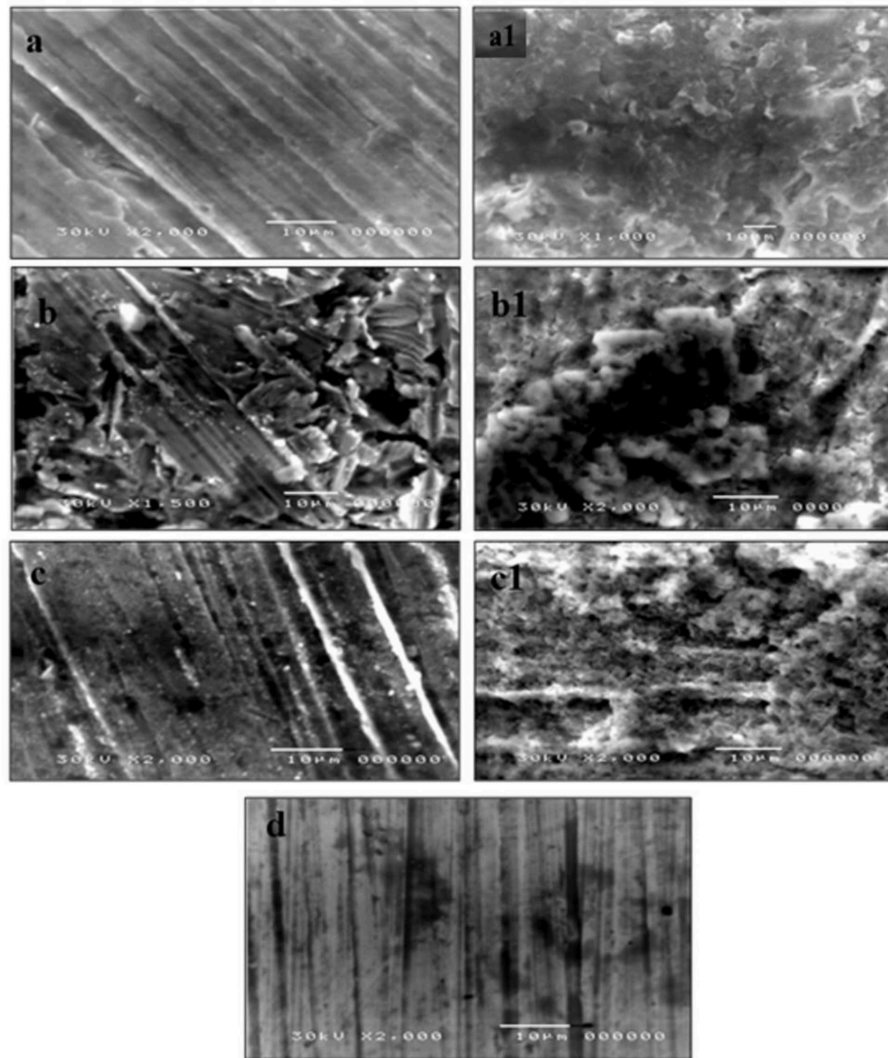


**FIGURE 6** | SEM images of coupons surface after treated with CuO/ZnO nanocomposite polymer for 18 h (a), 28 h (b), 48 h (c), and coupons surface after embedded in the strongest bio-corrosive strain *Proteus mirabilis1* for 18 h (a1), 28 h (b1), 48 h (c1), and (d), control.

from potential-dynamic polarization curves. The inhibition efficiency was significantly high and increased by increasing the nanocomposite concentration. The incorporation of nanoparticles in the polymeric thin layer can significantly progress their barrier performance by diminishing the penetrability and twisting the diffusion path for corrosive species such as oxygen and chloride anions ( $\text{Cl}^-$ ) (Cherpinski et al., 2018). Previous studies demonstrated that; incorporation of nanoparticles (e.g., polyaniline/ ferrite, ZnO,  $\text{Fe}_2\text{O}_3$ , hallo site clay, and other nanoparticles) into conventional polymer thin layer also significantly increases the anti-corrosive performance (Bian et al., 2013; Pacheco-Torgal et al., 2013).

It was notable that in the presence of the nanocomposite the values of  $i_{\text{corr}}$  are greatly decreased. As demonstrated in **Table 2**, the value of  $i_{\text{corr}}$  in the case of the nanocomposite is less ( $i_{\text{corr}} = 0.0233 \mu\text{A cm}^{-2}$ ) than the blank (HCl)

( $i_{\text{corr}} = 0.3035 \mu\text{A cm}^{-2}$ ) indicating high corrosion protection properties. The decrease in the corrosion current indicated the establishment of protective films on metal surfaces. The inhibition efficiencies (IE%) can be calculated from  $i_{\text{corr}}$  as follows:

$$\text{IE\%} = 1 - ((i_{\text{corr}})/(i_{\text{corr}}^{\circ})) \times 100 \quad (3)$$

where  $i_{\text{corr}}^{\circ}$  and  $i_{\text{corr}}$  are the uninhibited and the inhibited corrosion current densities, respectively. The addition of the nanocomposite to 1M HCl solution led to a slight alteration in the values of  $E_{\text{corr}}$  in the negative direction in contrast to the result obtained in the absence of the inhibitor (Özcan et al., 2008).

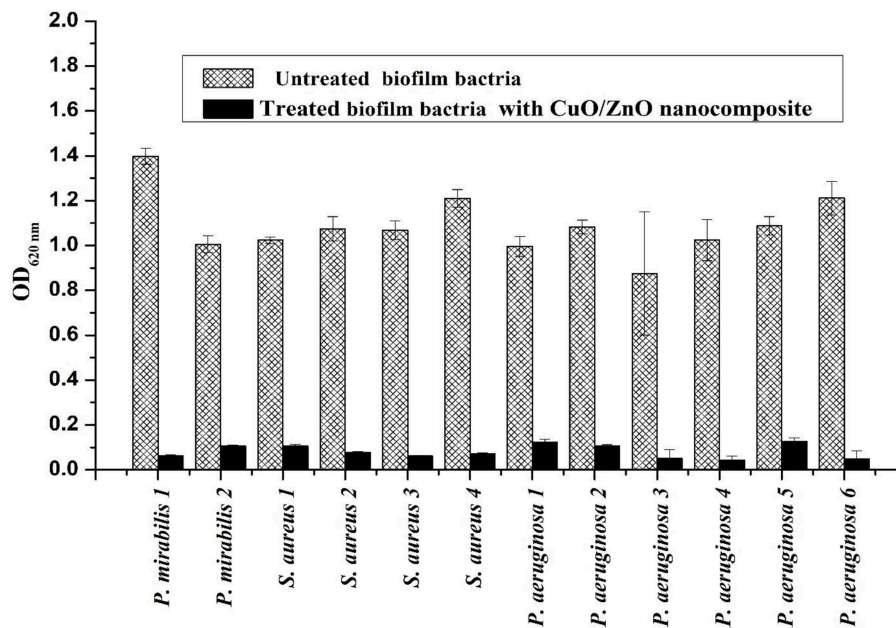


**FIGURE 7** | *Proteus mirabilis* (*P. mirabilis*), *Pseudomonas aeruginosa* (*P. aeruginosa*), and *Staphylococcus aureus* (*S. aureus*) biofilm formation and anti-biofilm effect of CuO/ZnO nanocomposite treatment.

**TABLE 1** | Bacterial strains hydrophobicity and CuO/ZnO nanocomposite polymer anti-hydrophobicity.

Bacterial strains	Hydrophobicity (%)	Anti-hydrophobicity in presence of nanocomposite polymer (%)
<i>Staphylococcus aureus</i> 1	40.53	22.23
<i>Staphylococcus aureus</i> 2	36.47	0.697
<i>Staphylococcus aureus</i> 3	90.47	3.13
<i>Staphylococcus aureus</i> 4	92.43	10.13
<i>Proteus mirabilis</i> 1	66.43	15.37
<i>Proteus mirabilis</i> 2	30.27	12.23
<i>Pseudomonas aeruginosa</i> 1	89.4	33.47
<i>Pseudomonas aeruginosa</i> 2	91.23	25.3
<i>Pseudomonas aeruginosa</i> 3	47.38	20.33
<i>Pseudomonas aeruginosa</i> 4	70.33	25.2
<i>Pseudomonas aeruginosa</i> 5	75.67	20.43
<i>Pseudomonas aeruginosa</i> 6	90.4	32.15

The alteration in corrosion potential values was in range  $\pm 85$  Mv thus indicates that nanocomposite plays a mixed type corrosion inhibitor toward the negative direction can be attributed to the strong influence of the nanocomposite on the oxygen cathodic reduction. It can be concluded that nanocomposite played as a mixed-type corrosion inhibitor (Figure 9) where anodic and cathodic reactions were diminished by obstructing the active sites on the steel surface (Elnaggar et al., 2015).

The electrochemical corrosion parameters such as, corrosion potential ( $E_{\text{corr}}$ ), corrosion current density ( $I_{\text{corr}}$ ), anodic ( $\beta_a$ ), and cathodic ( $\beta_c$ ) Tafel lines slopes were calculated from Tafel line fitted to the Sterne Geary equation using Gamry Echem Analyst software and the obtained results were depicted in the fraction of surface coverage ( $\theta$ ) and the inhibition activity

percentage ( $\eta\%$ ) according to  $I_{\text{corr}}$  values, are calculated from the following equations:

$$\theta = 1 - \left( \frac{i}{i^0} \right) \quad (4)$$

where,  $i^0$  and  $i$  are the corrosion current densities of tested steel prior to and after the addition of the tested nanocomposite corrosion inhibitors, respectively, indicate that the  $i$  values are significantly lower in the presence of the corrosion inhibitors compared to uninhibited solution. The corrosion current density decreases, upon incremental addition of the nanocomposite inhibitors (25–150 ppm) and with increasing the number of carbon atoms in the hydrophobic chain (Abd-Elaal et al., 2017).

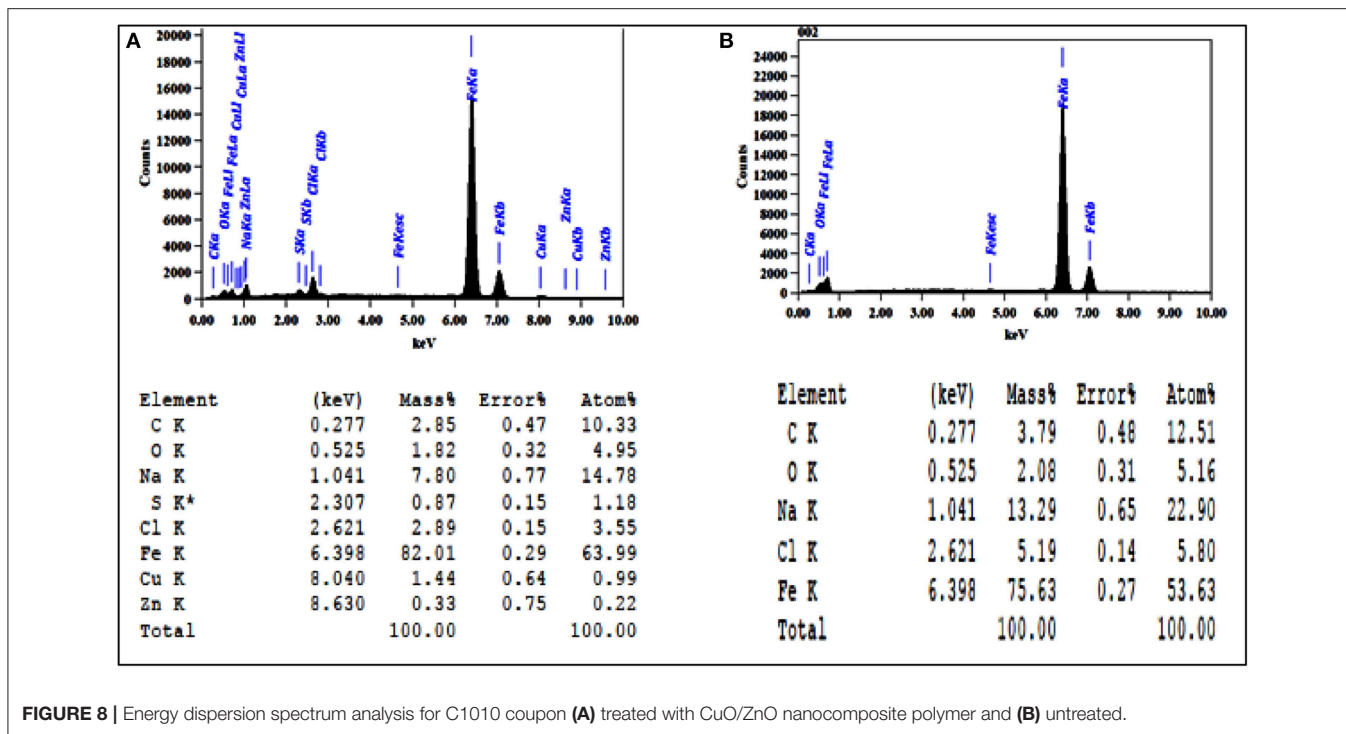


FIGURE 8 | Energy dispersion spectrum analysis for C1010 coupon (A) treated with CuO/ZnO nanocomposite polymer and (B) untreated.

## Electrochemical Impedance Spectroscopy

EIS measurements are used to confirm the above-mentioned electrochemical behavior and to study the characteristic capacitive properties at the mild steel/solution interface. Also, Figures 10, 11 represents the Nyquist and Bode plots of the nanocomposite tested sample in 1 M HCl in the absence and presence of different concentrations. From the EIS investigation could analyze all the diagrams obtained based on an equivalent circuit shown in Figure 10.  $R_s$  is the solution resistance,  $R_{ct}$  is the charge transfer resistance, and CPE is the constant phase element.

As shown in Figure 10 increasing the diameter of the semicircle in the Nyquist plots leads to the higher corrosion resistance of the surface layer. According to the Nyquist plot for carbon mild steel in 1 M HCl, blank, containing different concentrations of nanocomposite inhibitor (25–150 ppm) and the data in Table 3 list the impedance parameters of the Nyquist plots in different concentrations shows that, at a concentration of 150 ppm, the percentages of inhibition efficiency are highest when the charge transfer potential,  $R_{ct}$ , was decreased also in good agreement. In these spectra, the variation of impedance responses of mild steel after the addition of the nanocomposite in 1 M HCl solution is remarkable. The Randles CPE circuit was known as the equivalent circuit in our study (Figure 10). The increased protection indicated the significant contribution of the nanocomposite in maximizing the corrosion resistance of mild steel in 1 M HCl. Also, the width of the capacitive loop (represented as semicircles) was increased by increasing the concentration of the nanocomposite (de Melo et al., 2013).

The polymer film behaved like a barrier against the attack of the corrosive environment. The corresponding fitting results

are listed in Table 3, where the addition of nanocomposite increased the  $R_{ct}$  values proportional to the concentration. The values  $C_{dl}$  exhibited a declining tendency with increasing of the nanocomposite concentration. The results can be explained on the basis of the gradual replacement of water molecules by adsorption of the nanocomposite at the steel/solution interface and the establishment of a protective thin film of nanocomposite on the steel surface. The inhibition efficiency (IE%) can be calculated from the following equation:

$$IE\% = 1 - (R_{1ct})/(R_{2ct}) \times 100 \quad (5)$$

Where,  $R_{1ct}$  and  $R_{2ct}$  are the charge transfer resistances in the absence and presence of the nanocomposite, respectively.

The data presented in Table 3, reveal that  $R_{ct}$  values increased, while  $C_{dl}$  decreased, as the concentration of nanocomposite increase. The increasing  $R_{ct}$  values with the concentration, lead to reducing the exposed surface area of the mild steel electrode due to the formation of the adsorption protective thin layer film at the mild steel/solution interface. The  $C_{dl}$  values decrease compared to the untreated solution (1 M HCl) and further decrease with the increasing the nanocomposite inhibitor concentration. This can be described to the gradual substitution of the adsorbed water molecules at a mild steel surface by the synthesized nanocomposite particles, leading to the generation of a protective thin layer film on the mild steel surface, which resists the mass and charge transfers (Tao et al., 2012).

Bode plots of all the different nanocomposite concentration in 1 M HCl were shown in Figure 11. it gives the simultaneous measurement of modulus of impedance and phase angle with respect to frequency. The barrier property of a surface coating

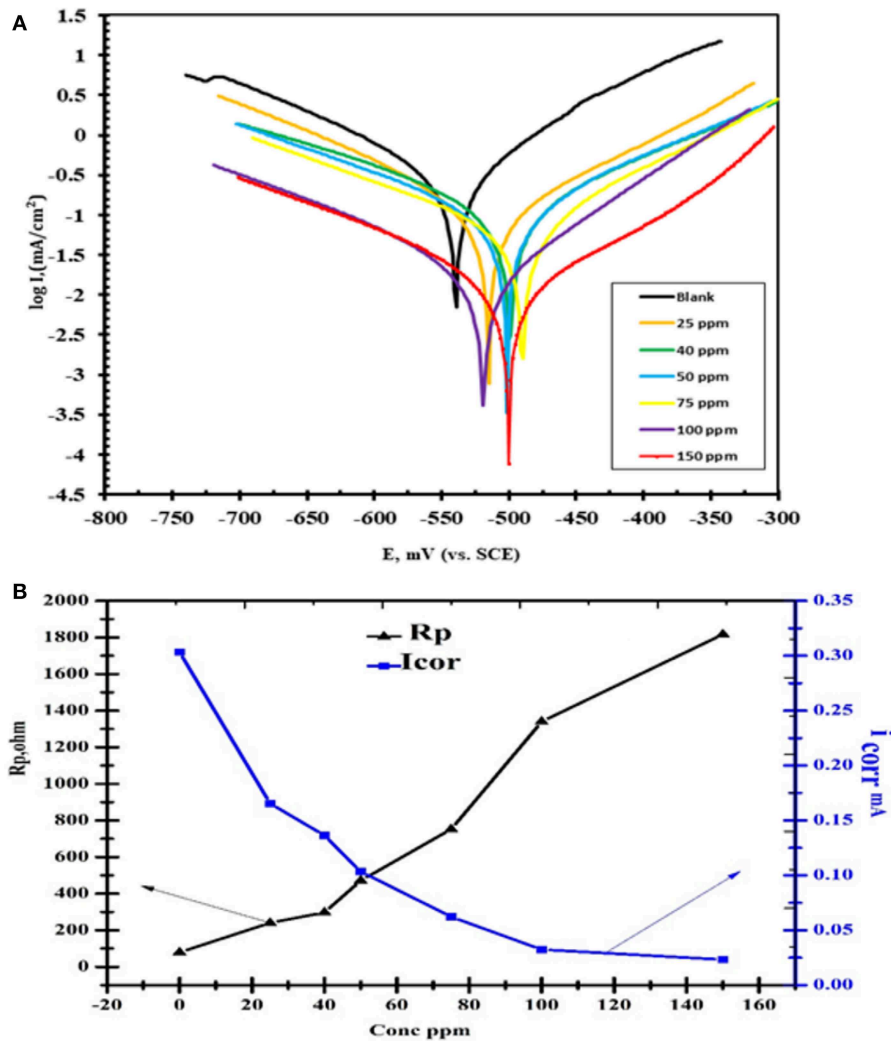


**FIGURE 9 | (A)** Polarization curves of concentrations CuO/ZnO nanocomposite polymer inhibitor for carbon steel in 1 M HCl at 25°C. **(B)** The polarization resistance (RP) and the corrosion current density ( $i_{corr}$ ).

can be investigated by the impedance magnitude in the low-frequency region with 100 and 150 ppm showed the high magnitude of impedances in this region which implies high pore resistance toward the electrolyte diffusion. It indicated that the presence of the nanocomposite polymer also increases the barrier protecting the ability for thin layer film.

The most interesting result is 150 ppm because value only decreases about 10 times from the beginning to the end

of nanocomposite and reach the maximum at the 150 ppm. It can be concluded that the higher the  $R_{ct}$ , the lower the steel corrosion rate and more efficient is the nanocomposite inhibitor. The EIS data matched with the data of Tafel techniques. The protection efficiency (92.31%) increased with increasing the concentration of the nanocomposite, the protection efficiency of the nanocomposite was calculated according to Medyalene et al. as follows; (Medyalene et al., 1995).

$$PE\% = \frac{ICorr. Rate (uncoated specimen) - ICorr. Rate (coated specimen)}{ICorr. Rate (uncoated specimen)} \times 100 \quad (6)$$

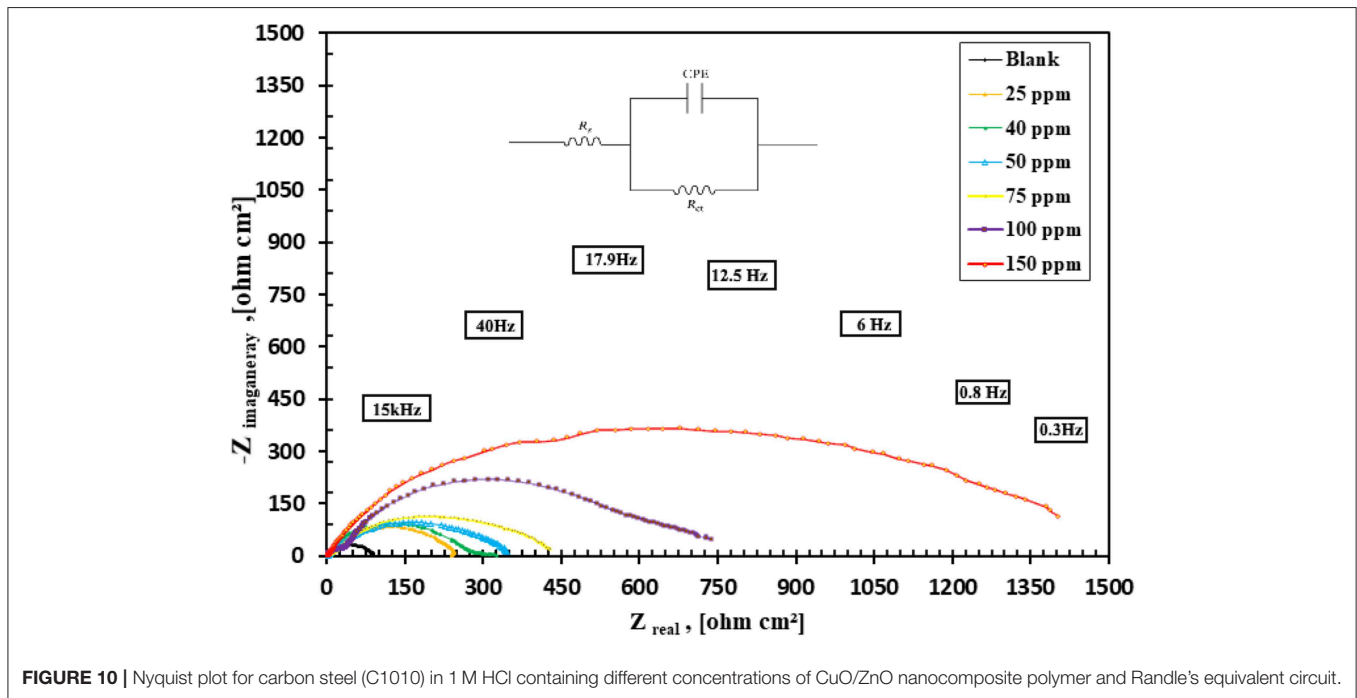
of immersion. The important changes in the shape of the Bode plot are respected to a function of exposure and the extended durability of the materials as demonstrated by the maintenance of high  $Z$ -values at low frequency at 1 M HCl. As in **Figure 11A** showed  $R_{ct}$  values increased with the increasing concentration

## Adsorption Isotherm

Adsorption isotherms are models used to represent the relationship between the amount of adsorbate (molecules) adsorbed by a given amount of adsorbent (steel surface) at a constant temperature. Many adsorption isotherms have been

**TABLE 2** | Potential-dynamic polarization parameters for corrosion of carbon steel in 1 M HCl in the absence and presence of different concentrations of CuO/ZnO nanocomposite polymer inhibitor at 25°C.

Inhibitor	Conc. ppm	$-E_{corr}$ (mV vs. SCE)	$-I_{corr}$ (mA m <sup>2</sup> )	$R_p$ ( $\Omega$ .cm <sup>2</sup> )	$\gamma_\alpha$ (mV dec <sup>-1</sup> )	$-\beta_c$ (mVdec <sup>-1</sup> )	Corr rate (mm/Y)	$\theta$	IE%
Blank HCl	–	539.5	0.3035	79.68	107.6	135.1	3.549	–	–
CuO/ZnO Nanocomposite polymer	25	539.5	0.1654	239.77	137.6	121.5	1.935	0.455	45.5
	40	514.9	0.1363	297.46	125.1	147.1	1.594	0.551	55.1
	50	551.3	0.1035	471.52	124.4	115.6	1.210	0.659	65.9
	75	513.7	0.0622	752.13	127.7	191.5	0.7272	0.795	79.5
	100	532.5	0.0324	1340.36	122.3	190.2	0.3787	0.893	89.3
	150	496.3	0.0233	1817.24	174.4	183.7	0.2726	0.923	92.3

**FIGURE 10** | Nyquist plot for carbon steel (C1010) in 1 M HCl containing different concentrations of CuO/ZnO nanocomposite polymer and Randle's equivalent circuit.

derived to explain the relationship between the surface coverage  $\theta$  and the pressure of the adsorbed molecules (Moudgil, 2010). As shown in **Figure 12**, the values of  $\Delta G$ , calculated according to Langmuir isotherm, were negative and are  $-10.95$  KJ/mol at 303 K and  $-12.58$  KJ/mol. These values indicated the adsorption of nanocomposite to be spontaneous and occur as physically. Generally, values of  $\Delta G$  up to  $-20$  KJ/mol signifies physical adsorption while values more than  $-40$  KJ/mol signifies chemical adsorption (Ikpi et al., 2012). The adsorption isotherm explained the anti-corrosion effect of the synthesized nanocomposite where the adsorption on the metal surface blocks the active sites or forms a protective barrier on mild steel surfaces. Khamis et al. had reported that the anti-corrosion effect of algae extracts has strong adsorption on the metal surface (Khamis et al., 2016).

From the calculated degree of surface coverage, it was possible to study different adsorption isotherms. Langmuir Isotherm Equation (7) which presented the best correlation coefficient in order to determine the adsorption characteristics of the

nanocomposite as a corrosion inhibitor as shown in **Figure 12**.

$$C/\theta = 1/K_{ads} + C \quad (7)$$

where:  $\theta$  is degree of surface coverage,  $C$  is the inhibitor concentration and  $k_{ads}$  is the equilibrium constant of the adsorption process.

The correlation coefficient obtained for the straight line was 0.9969 with an angular coefficient of 1.2037, suggesting the formation of a protective monolayer on the metal surface with a fixed number of adsorption sites. The angular coefficient is higher than 1. This deviation of Langmuir behavior suggests that the adsorbed molecules can occupy more than one active site (Ripper et al., 2016).

## CONCLUSION

In the present study, eco-friendly and low cost synthesized ZnO/CuO nanocomposite polymer was successfully obtained.

**TABLE 3** | EIS parameters for corrosion of carbon steel in 1 M HCl in the absence and presence of different concentrations of the synthesized CuO/ZnO nanocomposite polymer inhibitor at 25°C.

Inhibitor	Conc. (ppm)	$R_S$ ( $\Omega.cm^2$ )	$C_{dl}$ ( $\mu.F/cm^2$ )	$R_{ct}$ ( $\Omega.cm^2$ )	IE%
Blank	–	1.319	158.1	87.89	–
CuO/ZnO Nanocomposite polymer	25	1.553	54.23	243.3	63.88
	40	1.938	40.65	291.5	69.85
	50	1.694	34.49	348.4	74.744
	75	2.591	28.26	433.9	79.702
	100	2.785	18.56	711.7	87.651
	150	3.017	11.41	1448	93.930

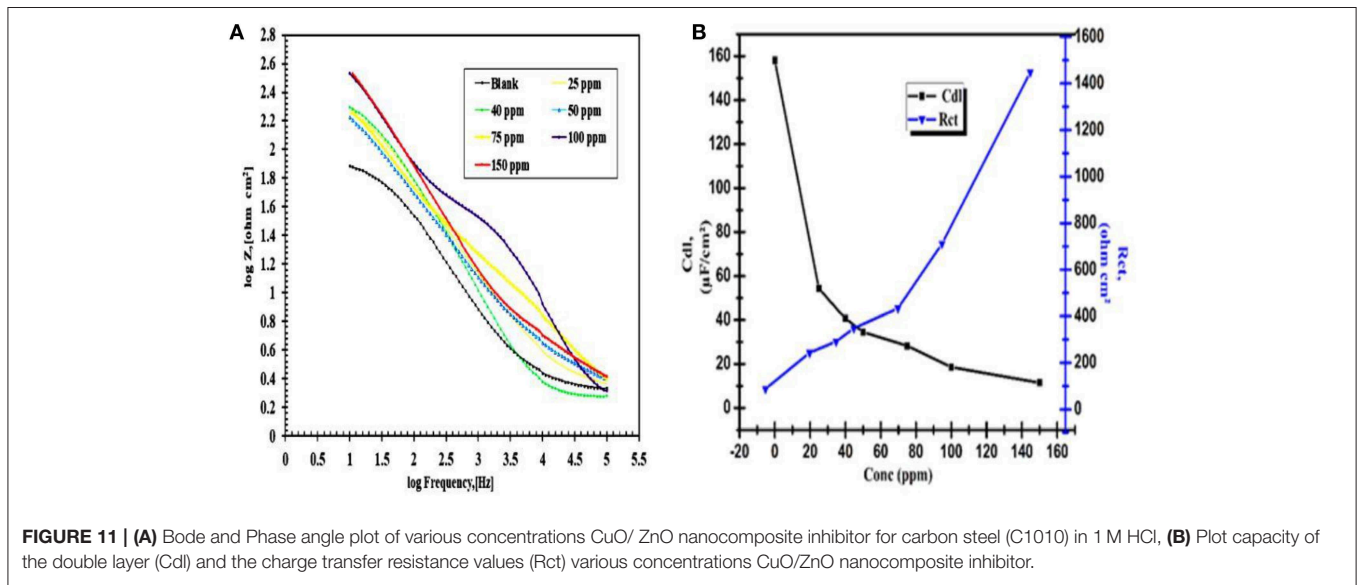


**FIGURE 11** | (A) Bode and Phase angle plot of various concentrations CuO/ ZnO nanocomposite inhibitor for carbon steel (C1010) in 1 M HCl, (B) Plot capacity of the double layer (Cdl) and the charge transfer resistance values (Rct) various concentrations CuO/ZnO nanocomposite inhibitor.

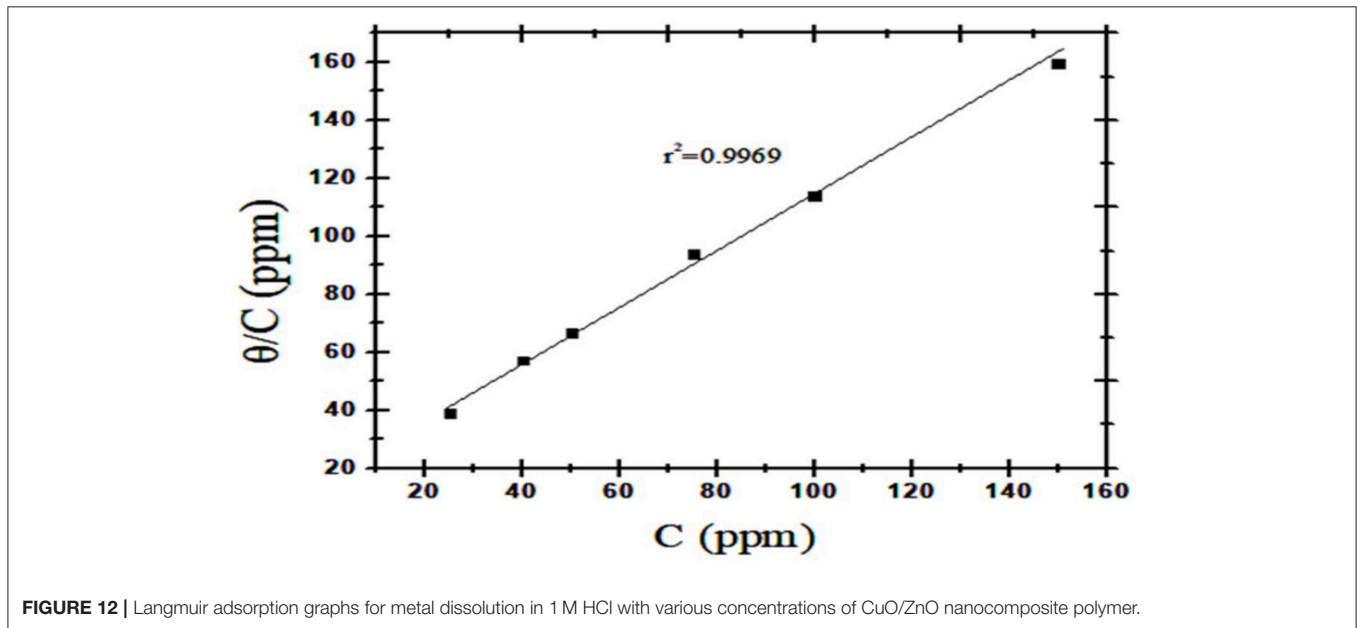


**FIGURE 12** | Langmuir adsorption graphs for metal dissolution in 1 M HCl with various concentrations of CuO/ZnO nanocomposite polymer.

The nanocomposite possessed anticorrosion potential in 1 M HCl. The protective performance and corrosion inhibition efficiency was 92.31%. The experimental data fitted the Langmuir adsorption isotherm. EDX- analysis confirmed that metal nanocomposite polymer was adsorbed onto the metal surface and formed a protective layer that inhibited the corrosion. Nanocomposite showed a potent inhibitor of biofilm formation moreover antibacterial for both Gram-positive and Gram-negative bacteria. Also, it had an anti-hydrophobicity effect on biocorrosive bacteria which enhanced protection efficacy as biocorrosion inhibition.

## DATA AVAILABILITY

All datasets generated for this study are included in the manuscript and/or the **Supplementary Files**.

## REFERENCES

- Abboud, Y., Saffaj, T., Chagraoui, A., El Bouari, A., Brouzi, K., Tanane, O., et al. (2014). Biosynthesis, characterization and antimicrobial activity of copper oxide nanoparticles (CONPs) produced using brown alga extract (*Bifurcaria bifurcata*). *Appl. Nanosci.* 4, 571–576. doi: 10.1007/s13204-013-0233-x
- Abd-Elaal, A. A., Elbasiony, N. M., Shaban, S., and Zaki, E. G. (2017). Studying the corrosion inhibition of some prepared nonionic surfactants based on 3-(4-hydroxyphenyl) propanoic acid and estimating the influence of silver nanoparticles on the surface parameters. *J. Mol. Liquids.* 249, 304–317. doi: 10.1016/j.molliq.2017.11.052
- Agarwal, H., Kumar, S. V., and Rajeshkumar, S. (2017). A review on green synthesis of zinc oxide nanoparticles-an eco-friendly approach. *Resour. Efficient Technol.* 3, 406–413. doi: 10.1016/j.refit.2017.03.002
- Aigbodion, V., and Fayomi, O. (2016). Surface characterization, mechanical properties and corrosion behaviour of ternary based Zn-ZnO-SiO<sub>2</sub> composite coating of mild steel. *J. Alloys Compd.* 654, 561–566. doi: 10.1016/j.jallcom.2015.09.090
- Aleem, A. (1993). *The Marine Algae of Alexandria, Egypt*. Alexandria: Alexandria University, 139.
- Aruliah, R., and Ting, Y.-P. (2014). Characterization of corrosive bacterial consortia isolated from water in a cooling tower. *ISRN Corrosion* 2014:803219. doi: 10.1155/2014/803219
- Azizi, S., Namvar, F., Mahdavi, M., Ahmad, M. B., and Mohamad, R. (2013). Biosynthesis of silver nanoparticles using brown marine macroalga, *Sargassum muticum* aqueous extract. *Materials* 6, 5942–5950. doi: 10.3390/ma6125942
- Azmy, N. A. N., Abdullah, H., Naim, N. M., Hamid, A. A., Shaari, S., and Mokhtar, W. H. M. W. (2014). Gamma irradiation effect on the structural, morphology and electrical properties of ZnO-CuO doped PVA nanocomposite thin films for *Escherichia coli* sensor. *Radiat. Phys. Chem.* 103, 108–113. doi: 10.1016/j.radphyschem.2014.05.025
- Banik, J., and Basumallick, S. (2017). Nanoparticle-assisted photo-Fenton reaction for photo-decomposition of humic acid. *Appl. Water Sci.* 7, 4159–4163. doi: 10.1007/s13201-017-0566-9
- Basu, S., Bose, C., Ojha, N., Das, N., Das, J., Pal, M., et al. (2015). Evolution of bacterial and fungal growth media. *Bioinformation* 11, 182–184. doi: 10.6026/97320630011182
- Batista, J. F., Pereira, R. F., Lopes, J. M., Carvalho, M. F., Feio, M. J., and Reis, M. A. (2000). *In situ* corrosion control in industrial water systems. *Biodegradation* 11, 441–448. doi: 10.1023/A:1011620023116
- Baumgarten, T., Sperling, S., Seifert, J., von Bergen, M., Steiniger, F., Wick, L., et al. (2012). Membrane vesicle formation as multiple stress response mechanism enhances cell surface hydrophobicity and biofilm formation of *Pseudomonas*

## AUTHOR CONTRIBUTIONS

All authors listed have made a substantial, direct and intellectual contribution to the work, and approved it for publication.

## ACKNOWLEDGMENTS

The authors would like to thank Professor Dr. Hassan Ahmed Abd-elrhim. Vice Chairman of the Egyptian Atomic Energy Commission for Scientific Research and Projects for the facilities provided for the author in this study.

## SUPPLEMENTARY MATERIAL

The Supplementary Material for this article can be found online at: <https://www.frontiersin.org/articles/10.3389/fmats.2019.00140/full#supplementary-material>

- putida* DOT-T1E cell surface hydrophobicity and biofilm formation. *Appl. Environ. Microbiol.* 78, 6217–6224. doi: 10.1128/AEM.01525-12
- Bian, L., Bao, L., Wang, J., and Lei, J. (2013). *In situ* preparation of monodispersed Ag/polyaniline/Fe<sub>3</sub>O<sub>4</sub> nanoparticles via heterogeneous nucleation. *Nanoscale Res. Lett.* 8:309. doi: 10.1186/1556-276X-8-309
- Bikiaris, D. N., and Triantafyllidis, K. S. (2013). HDPE/Cu-nanofiber nanocomposites with enhanced antibacterial and oxygen barrier properties appropriate for food packaging applications. *Mater. Lett.* 93, 1–4. doi: 10.1016/j.matlet.2012.10.128
- Bogdanović, U., Vodnik, V., Mitrić, M., Dimitrijević, S., Škapin, S., D., et al. (2015). Nanomaterial with high antimicrobial efficacy? copper/polyaniline nanocomposite. *ACS Appl. Mater. Interfaces* 7, 1955–1966. doi: 10.1021/am507746m
- Cherpinski, A., Gozutok, M., Sasmazel, H., Torres-Giner, S., and Lagaron, J. (2018). Electrospun oxygen scavenging films of poly (3-hydroxybutyrate) containing palladium nanoparticles for active packaging applications. *Nanomaterials* 8:469. doi: 10.3390/nano8070469
- Chitra, K., and Annadurai, G. (2013). Antimicrobial activity of wet chemically engineered spherical shaped ZnO nanoparticles on food borne pathogen. *Int. Food Res. J.* 20, 59–64. doi: 10.1155/2014/725165
- de Melo, E. F., Alves, K. G. B., Junior, S. A., and de Melo, C. (2013). Synthesis of fluorescent PVA/polypyrrole-ZnO nanofibers. *J. Mater. Sci.* 48, 3652–3658. doi: 10.1007/s10853-013-7159-2
- Eaton, A. D., Clesceri, L. S., Greenberg, A. E., Rice, E. W., and Franson, M. A. H. (2005). *Standard Methods for the Examination of Water and Wastewater*. American Public Health Association. 21:1600.
- Elnaggar, E. M., Elsherif, H. S., Migahed, M. A., and Saleh, A. (2015). Nano reactive polymer as Asphalt modifier for anticorrosion application. *J. Nanosci. Nanoeng.* 1, 9–17. doi: 10.21608/ABSB.2011.7028
- Faúndez, G., Troncoso, M., Navarrete, P., and Figueroa, G. (2004). Antimicrobial activity of copper surfaces against suspensions of *Salmonella enterica* and *Campylobacter jejuni*. *BMC Microbiol.* 4:19. doi: 10.1186/1471-2180-4-19
- Gu, T., Jia, R., Unsal, T., and Xu, D. (2019). Toward a better understanding of microbiologically influenced corrosion caused by sulfate reducing bacteria. *J. Mater. Sci. Technol.* 35, 631–636. doi: 10.1016/j.jmst.2018.10.026
- Hanemann, T., and Szabó, D. V. (2010). Polymer-nanoparticle composites: from synthesis to modern applications. *Materials* 3, 3468–3517. doi: 10.3390/ma3063468
- Ikpi, M., Udoh, I., Okafor, P. J., Ekpe, U., and Ebenso, E. (2012). Corrosion inhibition and adsorption behaviour of extracts from *Piper guineensis* on mild steel corrosion in acid media. *Int. J. Electrochem. Sci.* 7, 12193–12206. doi: 10.1155/2012/897430
- Jia, R., Unsal, T., Xu, D., Lekbach, Y., and Gu, T. (2019). Microbiologically influenced corrosion and current mitigation strategies: a state of the art review. *Int. Biodeter. Biodegrad.* 137, 42–58. doi: 10.1016/j.ibiod.2018.11.007

- Joshi, R., Hareesh, K., Bankar, A., Sanjeev, G., Asokan, K., Kanjilal, D., et al. (2017). Anti-biofilm efficacy of 100 MeV gold ion irradiated polycarbonate against *Salmonella typhi*. *Radiat. Phys. Chem.* 141, 149–154. doi: 10.1016/j.radphyschem.2017.07.002
- Karthik, K., Jaya, N. V., Kanagaraj, M., and Arumugam, S. (2011). Temperature-dependent magnetic anomalies of CuO nanoparticles. *Solid State Commun.* 151, 564–568. doi: 10.1016/j.ssc.2011.01.008
- Khamis, E., El-Rafey, E., Abdel Gaber, A. M., Hefnawy, A., El-Din, N. S., and El-Din Esmail Ahmed, M. S. (2016). Comparative study between green and red algae in the control of corrosion and deposition of scale in water systems. *Desalination Water Treat.* 57, 23571–23588. doi: 10.1080/19443994.2015.1135480
- Lgaz, H., Bhat, K. S., Salghi, R., Jodeh, S., Algarra, M., Hammouti, B., et al. (2017). Insights into corrosion inhibition behavior of three chalcone derivatives for mild steel in hydrochloric acid solution. *J. Mol. Liquids* 238, 71–83. doi: 10.1016/j.molliq.2017.04.124
- Li, K., Whitfield, M., and Van Vliet, K. J. (2013). Beating the bugs: roles of microbial biofilms in corrosion. *Corrosion Rev.* 31, 73–84. doi: 10.1515/corrrev-2013-0019
- Little, B., Ray, R., Wagner, P., Jones-Meehan, J., Lee, C., and Mansfeld, F. (1991). Spatial relationships between marine bacteria and localized corrosion on polymer coated steel. *Biofouling* 13, 301–321.
- Little, B. J., and Lee, J. S. (2014). Microbiologically influenced corrosion: an update. *Int. Mater. Rev.* 59, 384–393. doi: 10.1179/1743280414Y.0000000035
- Little, B. J., and Lee, J. S. (2007). *Microbiologically Influenced Corrosion*. John Wiley and Sons, Inc. doi: 10.1002/047011245x
- Lou, Y., Lin, L., Xu, D., Zhao, S., Yang, C., Liu, J., et al. (2016). Antibacterial ability of a novel Cu-bearing 2205 duplex stainless steel against *Pseudomonas aeruginosa* biofilm in artificial seawater. *Int. Biodeteriorat. Biodegrad.* 110, 199–205. doi: 10.1016/j.ibiod.2016.03.026
- Mathur, T., Singhal, S., Khan, S., Upadhyay, D., Fatma, T., and Rattan, A. (2006). Detection of biofilm formation among the clinical isolates of staphylococci: an evaluation of three different screening methods. *Indian J. Med. Microbiol.* 24, 25–29. doi: 10.4103/0255-0857.19890
- Medyalene, V. V., Leinartas, K. K., and Zyzyalyunas, E. E. (1995). Corrosion behaviour of composite nickel coatings in sulfuric acid solutions. *Zashch. Met.* 31, 98–100.
- Moen, B., Røssvoll, E., Måge, I., Møretro, T., and Langsrud, S. (2015). Microbiota formed on attached stainless steel coupons correlates with the natural biofilm of the sink surface in domestic kitchens. *Can. J. Microbiol.* 62, 148–160. doi: 10.1139/cjm-2015-0562
- Moudgil, H. K. (2010). *Textbook of Physical Chemistry*. Prentice-Hall Of India Pvt. Limited. Available online at: <https://books.google.com.eg/books?id=PBJO2NXEbaAC>
- Muñoz-Bonilla, A., and Fernández-García, M. (2012). Polymeric materials with antimicrobial activity. *Prog. Polym. Sci.* 37, 281–339. doi: 10.1016/j.progpolymsci.2011.08.005
- Nakao, R., Ramstedt, M., Wai, S. N., and Uhlin, B. E. (2012). Enhanced biofilm formation by *Escherichia coli* LPS mutants defective in Hep biosynthesis. *PLoS ONE* 7:28. doi: 10.1371/journal.pone.0051241
- Nan, L., Xu, D., Gu, T., Song, X., and Yang, K. (2015). Microbiological influenced corrosion resistance characteristics of a 304L-Cu stainless steel against *Escherichia coli*. *Mater. Sci. Eng. C* 48, 228–234. doi: 10.1016/j.msec.2014.12.004
- Özcan, M., Karadag, F., and Dehri, I. (2008). Investigation of adsorption characteristics of methionine at mild steel/sulfuric acid interface: an experimental and theoretical study. *Colloids Surf. A Physicochem. Eng. Aspects* 316, 55–61. doi: 10.1016/j.colsurfa.2007.08.023
- Pacheco-Torgal, F., Diamanti, M. V., Nazari, A., and Goran-Granqvist, C. (2013). *Nanotechnology in Eco-Efficient Construction: Materials, Processes and Applications*. Elsevier, Woodhead Publishing. Available online at: <https://www.sciencedirect.com/book/9780857095442/nanotechnology-in-eco-efficient-construction#book-info>
- Paik, J. K., and Melchers, R. E. (2014). *Condition Assessment of Aged Structures*. Cambridge, UK: Elsevier.
- Palazzo, A. (2016). *The Impact of Fluoride on the Corrosivity of Brackish Water on Mild Steel in Industrial Cooling Water Systems*. Ph. D. Dissertation, University of the Witwatersrand, Johannesburg, 5–48.
- Palza, H. (2015). Antimicrobial polymers with metal nanoparticles. *Int. J. Mol. Sci.* 16, 2099–2116. doi: 10.3390/ijms16012099
- PraveenKumar, C. M., Venkatesha, T. V., Vathsala, K., and Nayana, K. O. (2012). Electrodeposition and corrosion behavior of Zn-Ni and Zn-Ni-Fe 2 O 3 coatings. *J. Coat. Technol. Res.* 9, 71–77. doi: 10.1007/s11998-011-9322-5
- Qamar, M. T., Aslam, M., Ismail, I. M., Salah, N., and Hameed, A. (2015). Synthesis, characterization, and sunlight mediated photocatalytic activity of CuO coated ZnO for the removal of nitrophenols. *ACS Appl. Mater. Interfaces* 7, 8757–8769. doi: 10.1021/acsami.5b01273
- Rajasekar, A., Babu, T. G., Maruthamuthu, S., Pandian, S. K., Mohanan, S., and Palaniswamy, N. (2007). Biodegradation and corrosion behaviour of *Serratia marcescens* ACE2 isolated from an Indian diesel-transporting pipeline. *World J. Microbiol. Biotechnol.* 23, 1065–1074. doi: 10.1007/s11274-006-9332-0
- Ripper, B. D., Perrone, D., and D'Elia, E. (2016). Roasted coffee extracts as corrosion inhibitors for mild steel in HCl solution. *Mater. Res.* 19, 1276–1285. doi: 10.1590/1980-5373-mr-2015-0740
- Rosenberg, M., and Rosenberg, E. (1985). Bacterial adherence at the hydrocarbon-water interface. *Oil Petrochem. Pollut.* 2, 155–162. doi: 10.1016/S0143-7127(85)90178-4
- Ruparelia, J. P., Chatterjee, A. K., Duttagupta, S. P., and Mukherji, S. (2008). Strain specificity in antimicrobial activity of silver and copper nanoparticles. *Acta Biomater.* 4, 707–716. doi: 10.1016/j.actbio.2007.11.006
- Saab, M., Dias, O., and Faqeer, F. (2005). “Damage mechanisms and corrosion control in a crude unit overhead line,” in *CORROSION 2005* (Houston, TX: NACE International).
- Sarker, S. D., Nahar, L., and Kumarasamy, Y. (2007). Microtitre plate-based antibacterial assay incorporating resazurin as an indicator of cell growth, and its application in the *in vitro* antibacterial screening of phytochemicals. *Methods* 42, 321–324. doi: 10.1016/j.ymeth.2007.01.006
- Sharma, S., Mudhoo, A., Khamis, E., and Jain, G. (2008). Green corrosion inhibitors: an overview of recent research. *J. Corrosion Sci. Eng* 1:14.
- Smith, K., Gould, K. A., Ramage, G., Gemmell, C., Hinds, J., and Lang, S. (2010). Influence of tigeicycline on expression of virulence factors in biofilm-associated cells of methicillin-resistant *Staphylococcus aureus*. *Antimicrob. Agents Chemother.* 54, 380–387. doi: 10.1128/AAC.01155-09
- Stepanović, S., Vuković, D., Hola, V., Di Bonaventura, G., Djukić, S., Cirković, I., et al. (2007). Quantification of biofilm in microtiter plates: overview of testing conditions and practical recommendations for assessment of biofilm production by staphylococci. *APMIS* 115, 891–899. doi: 10.1111/j.1600-0463.2007.apm\_630.x
- Sun, D., Babar Shahzad, M., Li, M., Wang, G., and Xu, D. (2015). Antimicrobial materials with medical applications. *Mater. Technol.* 30, B90–B95. doi: 10.1179/1753555714Y.0000000239
- Tao, Z., He, W., Wang, S., Zhang, S., and Zhou, G. (2012). A study of differential polarization curves and thermodynamic properties for mild steel in acidic solution with nitrophenyltriazole derivative. *Corrosion Sci.* 60, 205–213. doi: 10.1016/j.corsci.2012.03.035
- Tripathi, D. K., Ahmad, P., Sharma, S., Chauhan, D. K., and Dubey, N. K. (2017). *Nanomaterials in Plants, Algae, and Microorganisms: Concepts and Controversies, Volume 1*. Academic Press.
- Vargas, I., Fischer, D., Alsina, M., Pavissich, J., Pastén, P., and Pizarro, G. (2017). Copper corrosion and biocorrosion events in premise plumbing. *Materials* 10:1036. doi: 10.3390/ma10091036
- Wadood, H. Z., Rajasekar, A., Ting, Y.-P., and Sabari, A. N. (2015). Role of *Bacillus subtilis* and *Pseudomonas aeruginosa* on corrosion behaviour of stainless steel. *Arab. J. Sci. Eng.* 40, 1825–1836. doi: 10.1007/s13369-015-1590-4
- Wang, L., Hu, C., and Shao, L. (2017). The antimicrobial activity of nanoparticles: present situation and prospects for the future. *Int. J. Nanomed.* 12:1227. doi: 10.2147/IJN.S121956
- Wang, P., Xu, G., Bian, L., Zhang, S., and Song, F. (2006). Study on sterols from brown algae (*Sargassum muticum*). *Chin. Sci. Bull.* 51, 2520–2528. doi: 10.1007/s11434-006-2124-y
- Wang, Y., Lee, S., M., and Dykes, G. (2015). The physicochemical process of bacterial attachment to abiotic surfaces: challenges for

- mechanistic studies, predictability and the development of control strategies. *Crit. Rev. Microbiol.* 41, 452–464. doi: 10.3109/1040841X.2013.866072
- Wei, H., Ding, D., Wei, S., and Guo, Z. (2013). Anticorrosive conductive polyurethane multiwalled carbon nanotube nanocomposites. *J. Mater. Chem. A* 1, 10805–10813. doi: 10.1039/c3ta11966a
- Yeole, K., Mahajan, L., and Mhaske, S. (2015). Poly (o-anisidine)-MWCNT nanocomposite: synthesis, characterization and anticorrosion properties. *Polym. Composit.* 36, 1477–1485. doi: 10.1002/p.c.23054

**Conflict of Interest Statement:** The authors declare that the research was conducted in the absence of any commercial or financial relationships that could be construed as a potential conflict of interest.

Copyright © 2019 Sadek, Farrag, Abdelsalam, Keiralla, Raafat and Araby. This is an open-access article distributed under the terms of the Creative Commons Attribution License (CC BY). The use, distribution or reproduction in other forums is permitted, provided the original author(s) and the copyright owner(s) are credited and that the original publication in this journal is cited, in accordance with accepted academic practice. No use, distribution or reproduction is permitted which does not comply with these terms.